Rheol Acta (2002) 41: 541–548
DOI 10.1007/s00397-002-0243-1

ORIGINAL CONTRIBUTION

Maria N. Charalambides
Leonard Wanigasooriya
J.Gordon Williams

Biaxial deformation of dough using the bubble inflation technique. II. Numerical modelling

Received: 2 November 2001
Accepted: 28 January 2002
Published online: 7 May 2002

M.N. Charalambides (✉)
L. Wanigasooriya · J.G. Williams
Mechanical Engineering Department,
Imperial College of Science,
Technology and Medicine,
London SW7 2BX, UK
E-mail: m.charalambides@ic.ac.uk

Abstract In Part I the bubble inflation test was used to measure the stress-strain relationship of dough. A large disagreement was found between the stress-strain curve based on experimental data and the curve derived from Bloksma's analytical model. In Part II, a numerical simulation of the bubble inflation test is performed using Finite Element Analysis, in order to obtain further information regarding the accuracy of the analytical predictions. A hyperelastic model is assumed for the dough, with a strain energy potential described by the compressible form of the Mooney-Rivlin model. Four cases were investigated, corresponding to various combinations of material parameters of the Mooney-Rivlin model. The numerical results reinforce the conclusions drawn in Part I of the study, specifically that Bloksma's analysis of the bubble inflation could lead to large errors in the stress-strain curve. It was further concluded that the accuracy of the analysis was dependent on the material properties. For a neo-Hookean material, the analysis leads to accurate results. This is because, for this material, all the assumptions made in the analysis regarding the bubble shape, the material's incompressibility and the bubble wall thickness distribution are accurate.

Keywords Dough · Finite element analysis · Hyperelastic · Bubble inflation

Introduction

In Part I of this work (Charalambides et al. 2002), the bubble inflation test was used to measure the stress-strain relationship of dough. This test method, shown schematically in Fig. 1, is widely used to characterise the mechanical behaviour of dough in equi-biaxial tension. The derivations of Bloksma (1957), summarised in the Appendix, are usually employed to analyse the experimental data of pressure and bubble volume. The analysis is based on the following assumptions: i) the dough is incompressible, ii) the bubble is spherical and iii) each dough particle is shifted normally to itself during inflation. However, in Part I, it was found that this analysis led to large errors in the predicted stress-strain response due to the inaccuracy of the underlying assumptions. Analytical predictions for the strain and bubble wall thickness were compared to experimentally derived values and considerable differences were found. At the top of the bubble, the analytical strain was larger and the thickness was much smaller than the experimental values. These discrepancies led to very large errors in the stress data. In addition, the bubble wall thickness distribution was more uniform than the analytical predictions. It was decided that a finite element analysis be performed such that comparisons can be made between the analytical and numerical stress-strain data. This will provide further information regarding the accuracy of the analytical method. It was thought that such information is needed, as the experimental data were prone to a large scatter due to the complexity of the measurements as well as the variability of the material. A

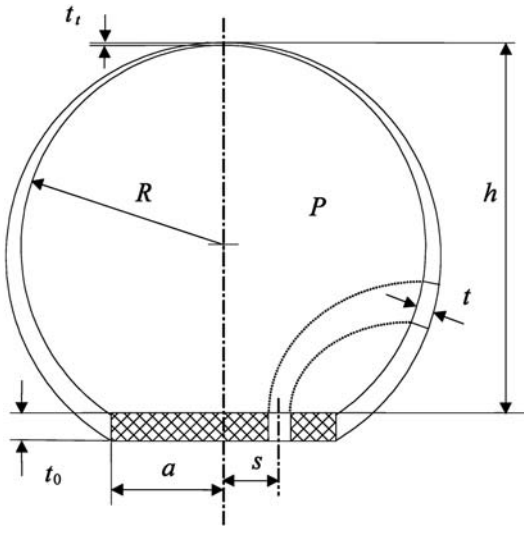

Fig. 1. Geometry of bubble inflation

detailed finite element analysis study would also aid in the deeper understanding of the problem as the effect of variations in material parameters on the test results can easily be quantified.

Model details

The commercially available Finite Element Analysis package ABAQUS (1998) was used. The standard implicit code was used. Eight-noded, axisymmetric, hybrid elements were used with 40 elements in the radial direction and one element through the thickness of the sample. The edge of the model was restricted to remain plane and was allowed to rotate around the middle node that was pinned.

A material model suitable for dough had to be chosen next. However, the mechanical properties of dough are of course the very purpose of the experiments and therefore are unknown. If a simple model were to be used with a small number of material parameters, it would be possible to perform an inverse identification numerical analysis, i.e. perform an iterative numerical study such that the material properties that lead to results agreeing with experimental readings of Part I are found. However, the tests were performed at constant inflation rate that led to a large variation in strain rate throughout the duration of the test (Charalambides et al. 2002; Rasper and Danihelkova 1986). As dough is a highly viscoelastic material, the variation in strain rate has a major effect on the stress-strain curve. In order to take into account this effect, a non-linear viscoelastic model ought to be used in the numerical analysis. Unfortunately, such a model involves a large number of material parameters, rendering the inverse identification numerical analysis impractical. Therefore, it was decided to use a simple hyperelastic model. The latter was developed to describe the behaviour of synthetic rubbery polymers that undergo large reversible strains and does not take into account the strain rate dependency of the material. Therefore, the numerical results cannot be directly compared with the experimental data of Part I. Nevertheless, the magnitudes of the material parameters will be chosen such that the numerical stresses are of the same order of magnitude as the experimental data, enabling a comparison between general trends. A comparison with the analytical predictions is of course still possible, which is the aim of this study.

The Mooney-Rivlin material model that is available in the ABAQUS software was used. The strain energy potential, W, is given by

$$W = C_{10}(\bar{I}_1 - 3) + C_{01}(\bar{I}_2 - 3) + \frac{1}{D_1}(J-1)^2 \tag{1}$$

where C_{10}, C_{01} and D_1 are the material properties to be determined. $\bar{I}_1$ and $\bar{I}_2$ are the first and second deviatoric strain invariants:

$$\bar{I}_1 = \bar{\lambda}_1^2 + \bar{\lambda}_2^2 + \bar{\lambda}_3^2 \text{ and } \bar{I}_2 = \bar{\lambda}_1^{(-2)} + \bar{\lambda}_2^{(-2)} + \bar{\lambda}_3^{(-2)} \tag{2}$$

The deviatoric stretches $\bar{\lambda}_i$ are related to the principal stretches λ_i (ratios of deformed to undeformed lengths) via

$$\bar{\lambda}_i = J^{-1/3}\lambda_i \tag{3}$$

and J is the volume ratio:

$$J = \lambda_1\lambda_2\lambda_3 \tag{4}$$

Note that for incompressible behaviour, J is equal to 1 and D_1 is equal to zero.

For a biaxial tension test

$$\lambda_1 = \lambda_2 = \lambda \text{ and } \sigma_{\text{eng}} = \frac{1}{2}\frac{\partial W}{\partial \lambda} \tag{5}$$

where σ_{eng} is the equi-biaxial engineering stress. The true stress σ is related to σ_{eng} by

$$\sigma = \sigma_{eng}\frac{\lambda}{J} \tag{6}$$

The initial shear modulus G and bulk modulus K are related to the material parameters via

$$G = 2(C_{10} + C_{01}) \quad K = \tfrac{2}{D_1} \tag{7}$$

In the special case where D_1 and C_{01} are both equal to zero, the strain energy function corresponds to the

neo-Hookean law. The equi-biaxial stress for this material is given by

$$\sigma = 2C_{10}\left(\lambda^2 - \frac{1}{\lambda^4}\right) \tag{8}$$

The constant C_{10} can be determined from a plot of σ vs (λ^2–λ^{-4}). In this study, such a plot was constructed with the analytical stress-strain data of Part I (Fig. 2). The strain ϵ is related to λ via

$$\varepsilon = \ln \lambda \tag{9}$$

From the slope of the line, C_{10} is calculated to be 367.4 Pa. Therefore the combination of $C_{10} = 367.4$, $C_{01} = D_1 = 0.0$ was used in the first numerical simulation (see Table 1). The effect of a non-zero C_{01} on the numerical results was determined through simulation 2 where the parameter was arbitrarily taken as 10 Pa. The effect of compressibility was evaluated in simulation 3, where C_{10} and C_{01} remained unchanged from simulation 2 and D_1 was set to 0.000274 Pa^{-1}. The latter implies an initial Poisson's ratio of 0.450. Finally, in simulation 4 which is also a compressible material, C_{01} was set to zero whereas C_{10} and D_1 remained unchanged from simulation 3. Note that the effect on the Poisson's ratio is minimal as it is only changed to 0.451. The four materials and the corresponding values of initial shear and bulk moduli as well as the Poisson's ratios are summarised in Table 1. The equi-biaxial stress-strain curves corresponding to the four materials are shown in Fig. 3.

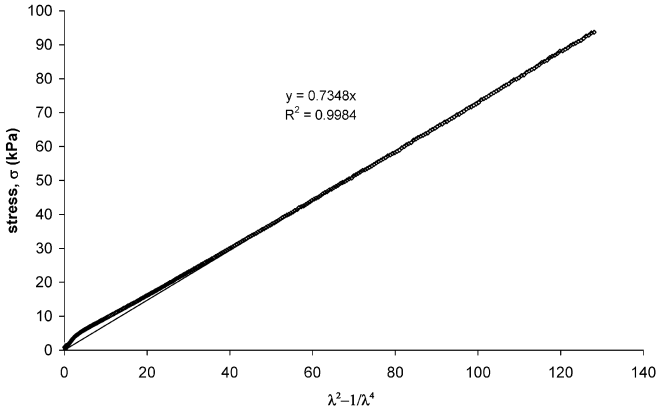

Fig. 2. Neo-Hookean model approximation

Results

The results from the numerical simulations corresponding to the four materials (see Table 1) will be presented next. First, for each simulation, the numerical stress and strain at the top of the bubble were compared to the material's actual stress-strain curve under equi-biaxial loading conditions. The comparison is shown in Fig. 4 for material 1. Excellent agreement is obtained, which is evidence that equi-biaxial conditions are prevailing at the top of the bubble. An excellent agreement was observed for the other three materials as well. Therefore, all numerical stress-strain data presented from now on represent the true material data.

The numerical data for pressure vs bubble height are shown in Fig. 5. The usual peak in pressure is observed, similar to experimental observations.

The strain at the top of the bubble is plotted vs bubble height in Figure 6. The analytical strain (Eq. A1) is also plotted such that a comparison can be made with the true, numerical values. It is observed that only material 1, the neo-Hookean material, leads to numerical results that are very close to the analytical data. This implies that for a neo-Hookean material, Bloksma's analysis would lead to the correct strain. This is not so for the other three materials where a clear disagreement is observed between the numerical and analytical values. It is of interest to note that for materials 2 and 3, the actual strain is lower than the analytical predictions, similar to the experimental observations in Part I. For material 4, however, the strain is larger than the analytical value.

The thickness, t_t, at the top of the bubble is plotted vs height in Fig. 7. Once again, the neo-Hookean material is the only material that leads to data that agree with Bloksma's analysis. Materials 2 and 3 lead to a larger thickness, similar to the experimental observations. Material 4 leads to values that are lower than the analytical values when the height exceeds approximately 60 mm.

The shape of the bubble corresponding to the four materials was also investigated. The ratio of the major to

Table 1. Materials used in numerical simulations and corresponding bubble shape

Simulation	C_{10} (Pa)	C_{01} (Pa)	D_1 (Pa^{-1})	G (kPa)	K (kPa)	v	k
1	367.4	0.0	0.0	0.73	∞	0.500	1.0
2	367.4	10.0	0.0	0.75	∞	0.500	1.1
3	367.4	10.0	0.000274	0.75	7.30	0.450	1.0
4	367.4	0.0	0.000274	0.73	7.30	0.451	0.9

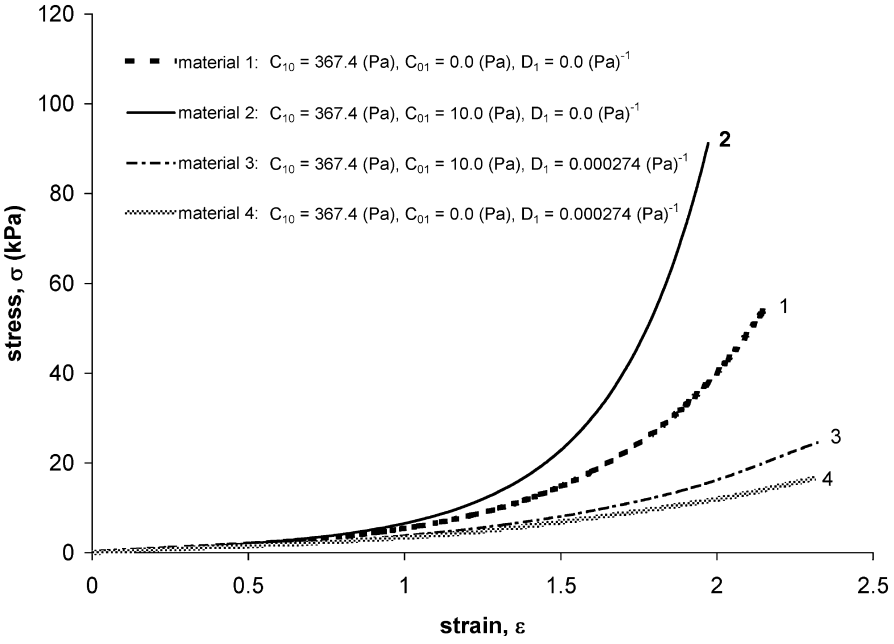

Fig. 3. Biaxial stress strain curves of four materials studied in numerical analysis

minor axes, k, was determined and is shown in Table 1. For a perfectly spherical bubble k is equal to unity. For values other than one, the bubble shape is elliptical. Values larger than one imply a bubble with a 'flattened' top whereas values smaller than one imply a bubble which is elongated in the vertical direction. From Table 1, it is apparent that the neo-Hookean material (material 1) and material 3 are spherical. For the other two materials, the bubble is elliptical.

Stress vs strain at the bubble top is plotted in Figs. 8, 9, 10 and 11 for materials 1 to 4 respectively. On each graph the numerical and analytical curves are shown. The analytical stress is calculated using Eqs. (A2), (A3) and (A4). For the compressible materials 3 and 4, an additional curve called 'semi-numerical' is plotted. For this curve, the numerical strains were used to calculate the wall thickness, assuming material incompressibility (Eq. A5). The latter assumption is of course invalid for materials 3 and 4 where D_1 is non-zero. This thickness was used in Eq. (A2) to calculate the stress. The corrected radius of curvature was used for the elliptical bubble of material 4 (Eq. A7).

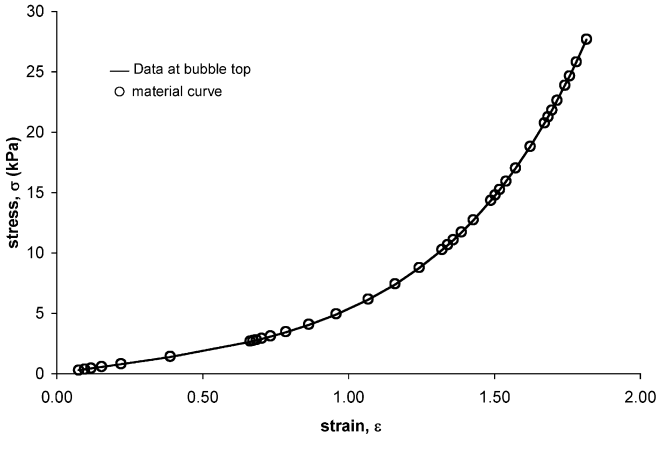

Fig. 4. Comparison of stress-strain at the top of the bubble with biaxial stress-strain curve for material 1 ($C_{10} = 367.4$ Pa, $C_{01} = 0.0$ Pa, $D_1 = 0.0$ Pa^{-1})

It is apparent that Bloksma's analysis leads to an accurate stress-strain curve only for the Neo Hookean material and in this case, the analytical and numerical curves coincide. This is in agreement with similar observations made by Williams (1980) in his analysis of rubber inflation. A small discrepancy, mainly in the stress, is apparent as the numerical curve seems to 'end' earlier than the analytical, i.e. the analytical prediction of the stress is approximately 10% higher than the true, numerical value. In contrast, Bloksma's analysis applied to material 2 data (Fig. 9) leads to a stress-strain curve that has a large discrepancy from the true curve. The stress at large strains, is overestimated by a factor of approximately 2.5 and the strain is also considerably overestimated (see Fig. 6).

The analysis also leads to large errors in the stress-strain curve for material 3 (Fig. 10). In contrast to the previous figure, the end result is that the analytical curve appears higher than the numerical curve. In addition, the assumption of incompressibility (semi-numerical) leads to a curve which is also in error, even though the stresses are reduced and the values become closer to the true numerical values. The errors in the stress are plotted vs bubble height in Fig. 12. At large

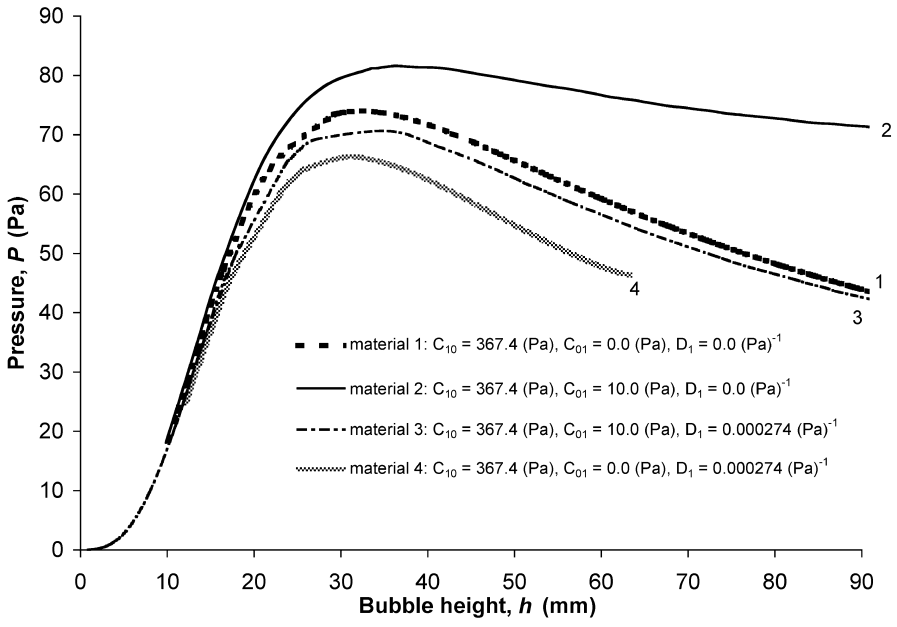

Fig. 5. Comparison of analytical and numerical pressure vs height data

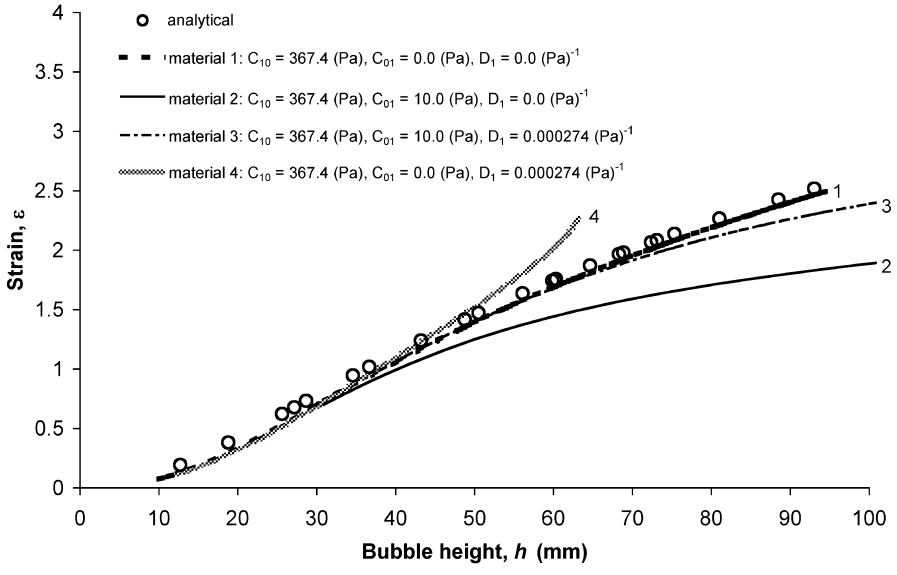

Fig. 6. Comparison of analytical and numerical strain at bubble top vs height data

heights the analysis is in error by approximately 440%. The assumption of incompressibility, even though it might sound reasonable for a material whose initial Poisson's ratio is 0.45, leads to errors of approximately 200% at large heights though the errors in the strain are much smaller (Fig. 13). This same trend was observed for the experimental data of Part I, reproduced in Fig. 14.

The numerical stress-strain curve is lower than the analytical predictions for material 4 (see Fig. 11). As was shown in Fig. 6, the strain is now underestimated by Bloksma's analysis, in contrast to the other three materials investigated. As a result, the thickness calculated from Eq. (A5) is smaller than the analytical value, thus increasing the stress and the error even further.

Finally, the numerical thickness distribution for material 3 when the bubble height is equal to 80 mm is plotted in Fig. 15. Material 3 was chosen as the analytical errors for this material followed the same trends as for the experimental study of Part I. The analytical prediction (Eq. A6) is also plotted. It is apparent that the numerical distribution is more uniform than the analytical one, once again agreeing with the experimental findings of Part I.

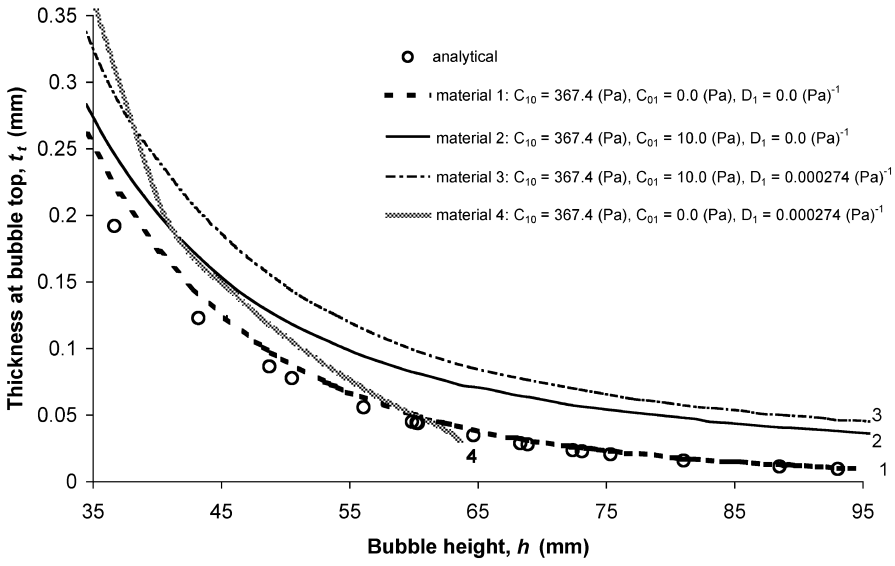

Fig. 7. Comparison of analytical and numerical thickness at bubble top vs height data

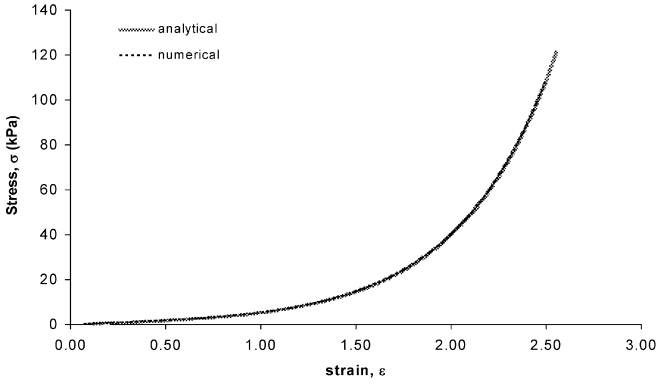

Fig. 8. Stress-strain curves for material 1 ($C_{10} = 367.4$ Pa, $C_{01} = 0.0$ Pa, $D_1 = 0.0$ Pa^{-1})

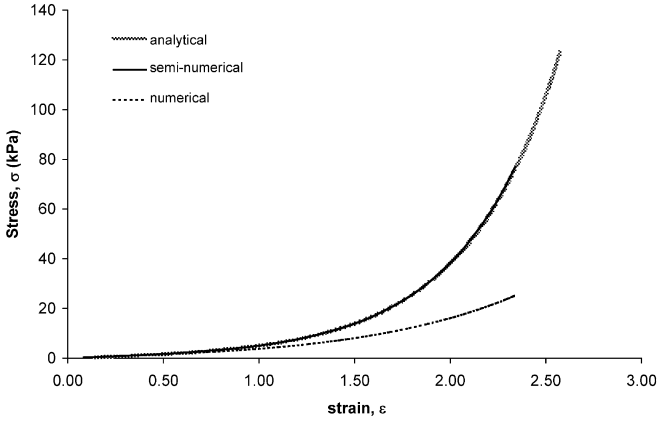

Fig. 10. Stress-strain curves for material 3 ($C_{10} = 367.4$ Pa, $C_{01} = 10.0$ Pa, $D_1 = 0.000274$ Pa^{-1})

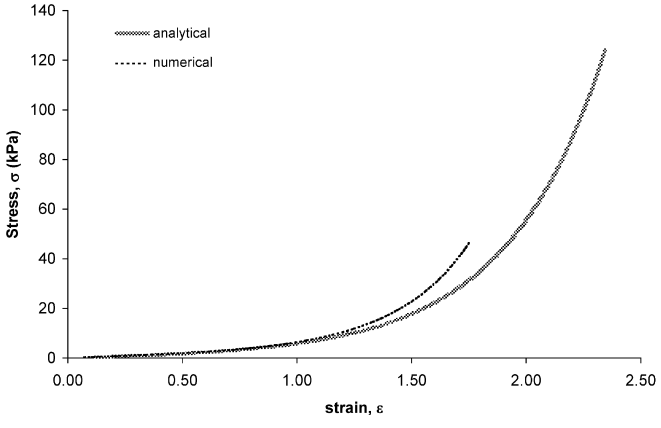

Fig. 9. Stress-strain curves for material 2 ($C_{10} = 367.4$ Pa, $C_{01} = 10.0$ Pa, $D_1 = 0.0$ Pa^{-1})

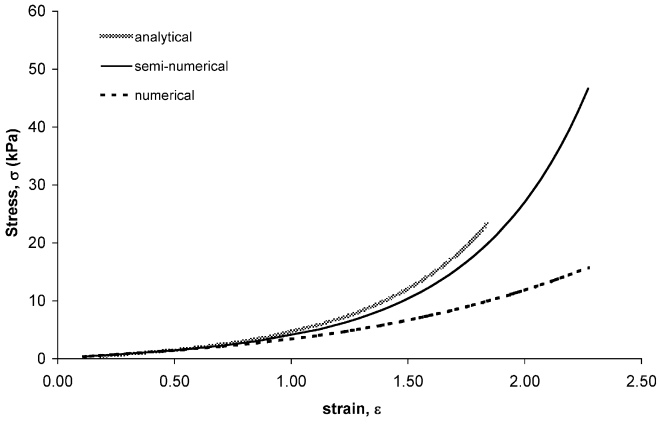

Fig. 11. Stress-strain curves for material 4 ($C_{10} = 367.4$ Pa, $C_{01} = 0.0$ Pa, $D_1 = 0.000274$ Pa^{-1})

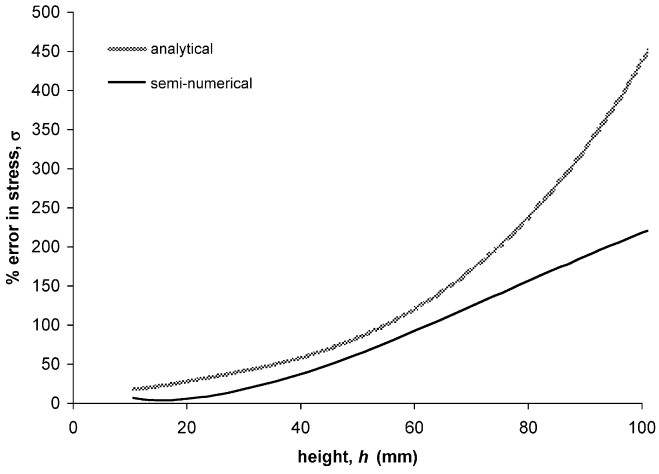

Fig. 12. Error in stress vs bubble height for material 3 ($C_{10} = 367.4$ Pa, $C_{01} = 10.0$ Pa, $D_1 = 0.000274$ Pa^{-1})

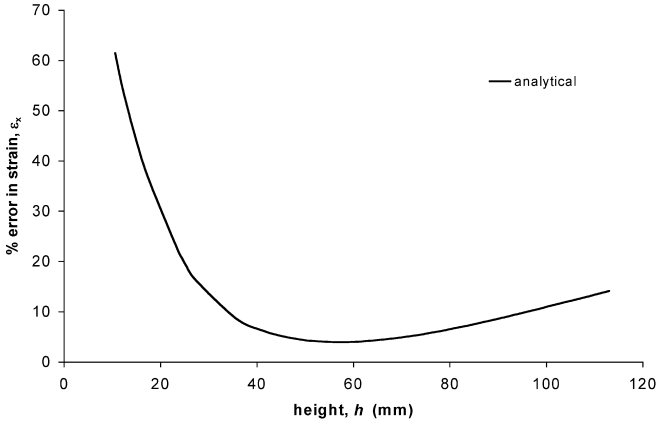

Fig. 13. Error in strain vs bubble height for material 3 ($C_{10} = 367.4$ Pa, $C_{01} = 10.0$ Pa, $D_1 = 0.000274$ Pa^{-1})

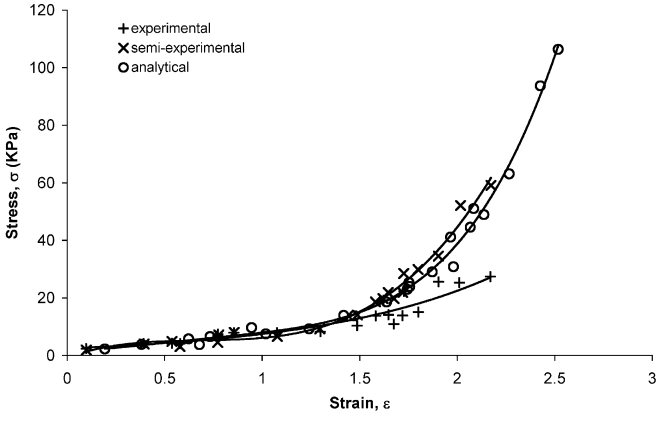

Fig. 14. Stress-strain curves reproduced from Part I of the study

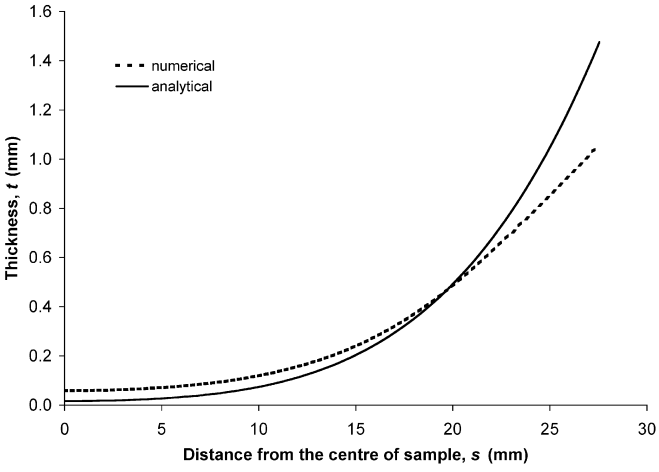

Fig. 15. Comparison of numerical and analytical bubble thickness distribution for material 3 ($C_{10} = 367.4$ Pa, $C_{01} = 10.0$ Pa, $D_1 = 0.000274$ Pa^{-1})

Conclusions

The numerical results reinforce the conclusions drawn in Part I of the study. Specifically, that, Bloksma's analysis of the bubble inflation test could lead to large errors in the calculated stress-strain curve. The accuracy of the analysis was dependent on the material properties. For a neo-Hookeian material, Bloksma's analysis leads to accurate results. This is because, for this material, all the assumptions made in the analysis regarding the bubble shape, the material's incompressibility and the bubble wall thickness distribution are accurate. However, for the other materials investigated in this study, the errors were very large. Specifically, the stress is largely overestimated whereas the strain is overestimated for some materials and underestimated for others. One particular material (material 3), led to very similar comparisons between numerical and analytical results to the comparisons between experimental and analytical results presented in Part I.

Even if the material is slightly compressible, i.e. the initial Poisson's ratio is in the region of 0.45, the incompressibility assumption will lead to large errors in the stress-strain curve. Therefore, care should be taken when assumptions regarding the compressibility of dough are made.

Since the purpose of the bubble inflation test is to determine the stress-strain curve and hence characterise the material, it will not be known, a priori, whether Bloksma's analytical method will lead to accurate results. Therefore, bubble height, strain and thickness as well as pressure need to be recorded during the test. In addition, efforts should be made to perform the test under constant strain rate by using a testing machine that is capable of adjusting the crosshead speed

according to the changes in the strain, via a feedback loop control system.

Acknowledgement The authors would like to acknowledge the financial support of General Mills, USA.

Appendix

The analysis by Bloksma (1957) leads to the following expressions for the planar strain, ϵ, and stress, σ, at the top of the inflated bubble:

$$\varepsilon = \ln\left(1 + \frac{h^2}{a^2}\right) \tag{A1}$$

$$\sigma = \frac{PR}{2t_t} \tag{A2}$$

where h is the bubble height, a the initial sample radius, P the pressure, t_t the thickness at the bubble top and R the bubble radius. The latter is calculated from

$$R = \frac{a^2 + h^2}{2h} \tag{A3}$$

The thickness at the top of the bubble is given by

$$t_t = t_0\left(1 + \frac{h^2}{a^2}\right)^{-2} \tag{A4}$$

where t_0 is the initial sample thickness. Alternatively, the thickness could also be calculated directly from known strain values assuming material incompressibility:

$$t_t = t_0 e^{-2e} \tag{A5}$$

The non-uniform distribution for thickness, t, along the bubble is described by

$$t = t_0\left[\frac{a^4 + s^2h^2}{a^2(a^2 + h^2)}\right]^2 \tag{A6}$$

Finally, the radius of curvature, R_c, for an elliptical bubble is given by

$$R_c = \frac{a^2 + k^2h^2}{2h} \tag{A7}$$

where k is the ratio of the major to the minor axes of the ellipse.

References

ABAQUS (1998) ABAQUS Version 5.8. Hibbit, Karlsson and Sorensen, USA

Bloksma AH (1957) A calculation of the shape of the alveograms of some rheological model substances. Cereal Chem 34:126–136

Charalambides MN, Wanigasooriya L, Williams JG, Chakrabarti S (2002) Biaxial deformation of dough using the bubble inflation technique. I. Experimental. Rheol Acta (submitted)

Rasper VF, Danihelkova H (1986) Alveography in fundamental dough rheology. In: Faridi H, Faubion JM (eds) Fundamentals of dough rheology. American Association of Cereal Chemists, St Paul, MN, pp 169–180

Williams JG (1980) Stress analysis for polymers. Ellis Horwood, Chichester, pp 231–245